

Article

# Geophysical Interpretation of Horizontal Fractures in Shale Oil Reservoirs Using Rock Physical and Seismic Methods

Zhiqi Guo , Wenxuan Gao and Cai Liu

College of Geoexploration Science and Technology, Jilin University, Changchun 130021, China; gaowx21@mails.jlu.edu.cn (W.G.); liucaicai@jlu.edu.cn (C.L.)

\* Correspondence: guozhiqi@jlu.edu.cn

**Abstract:** Horizontal fractures are one of the factors that significantly affect the ultimate productivity of shale oil reservoirs. However, the prediction of horizontal fractures by using seismic methods remains a challenge, which is due to the complex elastic and seismic responses that are associated with horizontal fractures. A framework that predicts horizontal fractures by seismic rock physical methods has been developed in the present study. A shale model is then proposed to quantify the shale elastic responses that are associated with the properties of the horizontal fractures. The modeling results that are based on the logging data validated the applicability of the proposed model, and the predicted fracture properties could be used to evaluate the development of horizontal fractures. According to the framework of the Poisson impedance, a horizontal fracture indicator is suggested to represent the logging-derived fracture density in terms of a combination of elastic properties. By using seismic-inverted elastic properties, the obtained indicator enabled an estimation of zones with the potential development of horizontal fractures. The established indicator showed a good correlation with the fracture density and could be used as an effective indicator in the prediction of horizontal fractures in shale oil reservoirs. Furthermore, seismic data applications show a consistency between the development of horizontal fractures and the production status of the boreholes. This result highlights the importance of horizontal fractures for the ultimate productivity and emphasizes the applicability of the proposed methods.

**Keywords:** shale oil reservoir; horizontal fractures; fracture density; rock physics model; seismic interpretation



**Citation:** Guo, Z.; Gao, W.; Liu, C. Geophysical Interpretation of Horizontal Fractures in Shale Oil Reservoirs Using Rock Physical and Seismic Methods. *Energies* **2023**, *16*, 7514. <https://doi.org/10.3390/en16227514>

Academic Editor: Mofazzal Hossain

Received: 7 October 2023

Revised: 3 November 2023

Accepted: 7 November 2023

Published: 9 November 2023



**Copyright:** © 2023 by the authors. Licensee MDPI, Basel, Switzerland. This article is an open access article distributed under the terms and conditions of the Creative Commons Attribution (CC BY) license (<https://creativecommons.org/licenses/by/4.0/>).

## 1. Introduction

As groundbreaking unconventional resources, the shale reservoirs are providing an ever-increasing amount of oil and gas around the world, and better understanding of shale microstructures will provide improved characterization of various shale reservoirs [1–4]. Successful predictions of sweet spots in shale reservoirs should consider areas that include an abundance of organic enrichments. These enrichments are indicated by various factors, such as the total organic carbon (TOC), the high brittleness of the shale rock that facilitates hydraulic fracturing, and the development of natural fractures.

Seismic methods have contributed to the characterization of such factors in shale reservoirs. By using logging data and seismic-inverted elastic properties, the TOC in the shale has been evaluated by its elastic properties. A low density or an elastic impedance usually corresponds to a high TOC [5–9]. Also, the brittleness of the shale rock has been estimated by its mechanical properties, such as Young's modulus and Poisson's ratio [10–13]. Other practical brittleness factors have also been suggested, which were based on the combination of mechanical properties and the Lamé coefficients derived from elastic properties [14,15]. In addition, vertical fractures that were associated with tectonic activities could be predicted by using various azimuthal seismic inversion methods based on the anisotropic shale model [16–23].

In particular, shale exhibits an intrinsic anisotropy that is represented as vertical transverse isotropy (VTI). It results from the anisotropy of clay particles, laminated microstructural fabrics, and layered distributions of minerals and organic matter [24–30]. Moreover, the horizontal fractures that are developed in the shale rock can further enhance the degree of VTI anisotropy of the shale. Early experimental investigations have shown that the opening and closing of the aligned fractures in the shale at different stresses can lead to variations in the anisotropy [31,32]. Recent experiments and core and outcrop observations have indicated that the presence of horizontal fractures in the shale can cause substantial anisotropy variations with loading stresses [33–35]. Geological studies have also confirmed the importance of horizontal fractures for sweet spot predictions in shale reservoirs [36–39]. Accordingly, some efforts have been made to predict the VTI anisotropy of the shale based on rock physical modeling using logging data [40]. Furthermore, seismic dispersion attributes were derived by using the frequency-dependent pre-stack seismic inversion method in the prediction of fluid-saturated bedding-parallel fractures [41]. Despite such efforts, it remains a challenge to predict horizontal fractures in the shale, which is due to the complex elastic and seismic responses of the bedding-aligned fractures.

Rock physical modeling can unravel the elastic characteristics of the shale, which are associated with various petrophysical properties. So far, numerous modeling methods have been developed to quantify the elastic responses and the corresponding seismic signatures of organic matter in the shale [14,24,27–29,32,42–45]. In addition, the shale anisotropy that is related to clay lamination and microstructural fabrics has been investigated by using modeling methods [43,46,47]. The shale brittleness has also been incorporated in the rock physical modeling for the prediction of engineering sweet spots in shale reservoirs [9,48]. However, shale models that quantify the effect of horizontal fractures on the shale elastic properties are rare. Further investigations are, therefore, needed to develop practical methods with which it is possible to predict horizontal fractures from logging data, in addition to seismic data that are based on the shale model.

In the present study, rock physical modeling and seismic methods are developed for the prediction of horizontal fractures in shale oil reservoirs. At first, a shale model is proposed for the description of elastic responses associated with horizontal fracture properties. As the next step, various horizontal fracture properties are estimated by using logging data and the established shale model. Based on the framework of the Poisson impedance, a horizontal fracture indicator is, thereafter, proposed to represent the logging-derived fracture density in terms of elastic properties. The obtained indicator is then applied to seismic data from a shale oil reservoir for a quantitative interpretation of the horizontal fractures from seismic-inverted elastic properties. Finally, the calculated results are compared with TOC and validated with the production status of the boreholes in the studied areas.

## 2. Methods

### 2.1. Rock Physics Model of Shale Oil Reservoirs

As shown in Figure 1, a framework for the modeling of shales has been proposed for the quantification of the effect of horizontal fractures on the shale elastic properties. At first, the theory of Hashin-Shtrikman (HS) bounds [49] was used to calculate equivalent elastic moduli of the shale solid matrix. According to the core analyses, the shale matrix is mainly composed of clay, quartz, calcite, and kerogen. In the modeling, the organic kerogen material was treated as a part of the solid matrix. Furthermore, the elastic moduli of the porous shale matrix were obtained by using the self-consistent approximation (SCA) theory [50], which considered the effect of fluid-filled matrix pores. Finally, the Hudson model [51] was used to add fluid-filled horizontal fractures to the porous matrix to obtain elastic properties of the shale rock. Specifically, in the proposed modeling method, the total porosity ( $\phi$ ) was considered as pore spaces that consisted of matrix pores ( $\phi_m$ ) and horizontal fractures ( $\phi_f$ ) (Figure 2). In addition, fluid mixtures of water and oil were assumed to be homogeneously

distributed in the matrix pores and horizontal fractures [52]. The rock physical theories that were used in the modeling are described in the following sections.

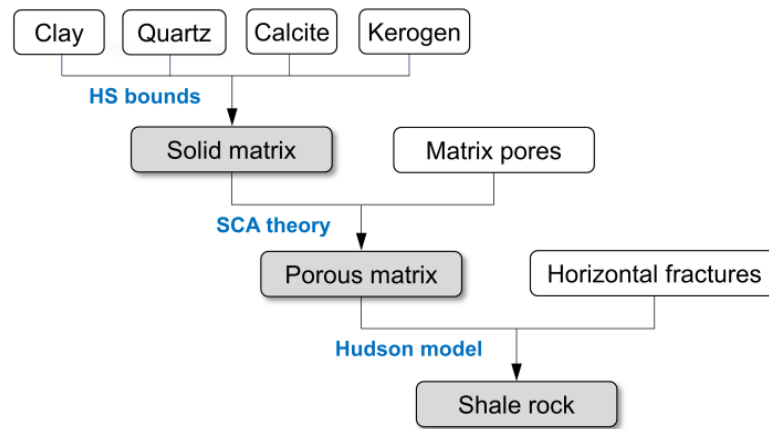


Figure 1. Flowchart of rock physical modeling for shale oil reservoirs.

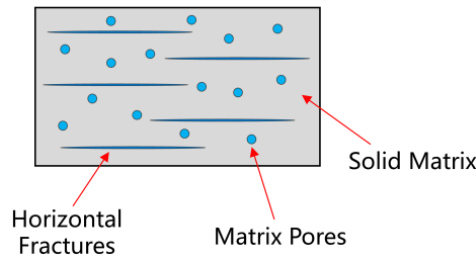


Figure 2. Schematics of the pore spaces in the shale matrix, which consist of matrix pores and horizontal fractures.

2.2. Hashin-Shtrikman Bounds

Hashin and Shtrikman (1963) [49] proposed a method to predict the equivalent elastic moduli of a mixture of mineral particles (Equation (1)):

$$\begin{aligned}
 K^{HS\pm} &= K_1 + \frac{f_2}{(K_2 - K_1)^{-1} + f_1(K_1 + \frac{4}{3}\mu_1)^{-1}} \\
 \mu^{HS\pm} &= \mu_1 + \frac{f_2}{(\mu_2 - \mu_1)^{-1} + \frac{2f_1(K_1 + 2\mu_1)}{5\mu_1(K_1 + \frac{4}{3}\mu_1)}}
 \end{aligned}
 \tag{1}$$

where  $K^{HS\pm}$  and  $\mu^{HS\pm}$  represent the narrowest upper and lower limits of bulk and shear modulus of the mixture consisting of two or more mineral phases, respectively.  $K_i$  and  $\mu_i$  represent the bulk and shear moduli, respectively, of each component. Also,  $f_i$  is the volume fraction component.

When the mixture has more than two types of mineral particles, the equivalent elastic moduli could be expressed in a general form (Equation (2)):

$$\begin{aligned}
 K^{HS+} &= \Lambda(\mu_{\max}), K^{HS-} = \Lambda(\mu_{\min}) \\
 \mu^{HS+} &= \Gamma[\zeta(K_{\max}, \mu_{\max})], \mu^{HS-} = \Gamma[\zeta(K_{\min}, \mu_{\min})]
 \end{aligned}
 \tag{2}$$

where

$$\begin{aligned}
 \Lambda(z) &= \left\langle \frac{1}{K(r) + \frac{4}{3}z} \right\rangle - \frac{4}{3}z \\
 \Gamma(z) &= \left\langle \frac{1}{\mu(r) + z} \right\rangle^{-1} - z \\
 \zeta(K, \mu) &= \frac{\mu}{6} \left( \frac{9K + 8\mu}{K + 2\mu} \right)
 \end{aligned}
 \tag{3}$$

where  $K(r)$  and  $\mu(r)$  represent the bulk and shear modulus corresponding to the  $r$ 'th component of the solid matrix;  $z$  represents the corresponding argument in Equation (2). The  $\langle \cdot \rangle$  bracket denotes the volumetric average of each component.

### 2.3. Self-Consistent Approximation Theory

Berryman (1980) [50] presented the SCA theory for an equivalent medium. A method was presented to calculate the elastic moduli of a model composed of multiphase minerals and pore spaces. The corresponding equations were represented in Equation (4):

$$\begin{aligned} \sum_{i=1}^N x_i (K_i - K_{SC}^*) P^{*i} &= 0 \\ \sum_{i=1}^N x_i (\mu_i - \mu_{SC}^*) Q^{*i} &= 0 \end{aligned} \quad (4)$$

where  $K_{SC}^*$  and  $\mu_{SC}^*$  are the equivalent bulk and shear modulus of the entire rock, respectively. The subscript  $i$  represents each mineral phase or pore space, and  $x_i$  represents the volume fraction of each phase. Also,  $K_i$  and  $\mu_i$  represent the bulk modulus and shear modulus, respectively, for each phase. The superscript  $*i$  of  $P$  and  $Q$  is the geometric factor for the inclusion material  $i$ . Furthermore, the coefficients  $P^{*i}$  and  $Q^{*i}$  represent the geometries of the inclusions.

### 2.4. Hudson Model

Hudson (1981) [51] established a penny-shaped microfracture model for the calculations of stiffness coefficients for a rock embedded with parallel microfractures (Equation (5)):

$$c_{ij} = c_{ij}^0 + c_{ij}^1 \quad (5)$$

where  $c_{ij}^0$  represents the elastic stiffness matrix of the host medium, and  $c_{ij}^1$  represents the first-order disturbances by the microfractures. The corresponding equations were presented in Equation (6):

$$\begin{aligned} c_{11}^1 &= -\frac{\lambda^2}{\mu} \varepsilon_f U_3 \\ c_{13}^1 &= -\frac{\lambda(\lambda+2\mu)}{\mu} \varepsilon_f U_3 \\ c_{33}^1 &= -\frac{\lambda(\lambda+2\mu)^2}{\mu} \varepsilon_f U_3 \\ c_{44}^1 &= -\mu \varepsilon_f U_1 \\ c_{66}^1 &= 0 \end{aligned} \quad (6)$$

where  $\lambda$  and  $\mu$  represent the Lamé constants of the host medium. Also,  $U_1$  and  $U_3$  depend on the states of the microfractures, and  $\varepsilon_f$  is the fracture density (Equation (7)):

$$\varepsilon_f = \frac{3\phi_f}{4\pi\alpha} \quad (7)$$

where  $\phi_f$  and  $\alpha$  represent the fracture porosity and the aspect ratio, respectively.

The definitions of the fluid-filled fractures were presented in Equation (8):

$$\begin{aligned} U_3 &= \frac{4(\lambda+2\mu)}{3(\lambda+\mu)} \frac{1}{1+\kappa} \\ U_1 &= \frac{16(\lambda+2\mu)}{3(3\lambda+4\mu)} \end{aligned} \quad (8)$$

where  $\kappa$  is the parameter that is used to describe the fracture characteristics (Equation (9)):

$$\kappa = \frac{K_f(\lambda+2\mu)}{\pi\alpha\mu(\lambda+\mu)} \quad (9)$$

where  $K_f$  represents the fluid bulk modulus.

### 2.5. Domenico Equation for the Fluid Mixture

Domenico (1977) [52] proposed a method for calculations of the bulk moduli of fluid mixtures. In the modeling of the shale oil reservoirs in our paper, the fluids were assumed to be a mixture of oil and water, homogeneously distributed in the spaces of matrix pores and horizontal fractures. The modulus of the mixed fluid was estimated by using Equation (10):

$$K_f = S_w K_w + S_o K_o \quad (10)$$

where  $K_w$  and  $K_o$  represent the moduli of water and oil, respectively, and the corresponding saturations of water and oil are represented by  $S_w$  and  $S_o$ , respectively.

Also, the density of the mixed fluid was calculated by using Equation (11):

$$\rho_f = S_w \rho_w + S_o \rho_o \quad (11)$$

where  $\rho_w$  and  $\rho_o$  represent water and oil density, respectively.

### 2.6. Prediction of the Horizontal Fracture Properties by Using the Shale Model and Logging Data

The proposed model for the shale oil reservoir (Figure 1) was used to develop a method for the estimation of horizontal fractures based on a model-based framework. By using well-log data, the shale model acted as a modeling tool in the prediction of the horizontal fracture density,  $\varepsilon_f$  (Figure 2). Specifically, the volumetric fractions and moduli of the minerals, kerogen, and fluids were as input data for modeling P-wave and S-wave velocities (i.e.,  $V_{P\text{-calculated}}$  and  $V_{S\text{-calculated}}$ ) for a set of preset values of horizontal fracture porosities ( $\phi_f$ ) and aspect ratios ( $\alpha$ ). An objective function (Equation (12)) was, thereafter, constructed to find the optimized values of ( $\phi_f, \alpha$ ) by minimizing the difference between  $V_{P\text{-calculated}}$  and  $V_{S\text{-calculated}}$  and the corresponding measured values (i.e.,  $V_{P\text{-measured}}$  and  $V_{S\text{-measured}}$ ) in the borehole:

$$f(\phi_f, \alpha) = \min \left( \left| V_{P\text{-calculated}}(\phi_f, \alpha) - V_{P\text{-measured}} \right|^2 + \left| V_{S\text{-calculated}}(\phi_f, \alpha) - V_{S\text{-measured}} \right|^2 \right) \quad (12)$$

Based on Equation (12), a simple grid-searching method has in the present study been used to find the optimized values of  $\phi_f$  and  $\alpha$ . According to Equation (7), the estimated  $\phi_f$  and  $\alpha$  values were finally used to compute the fracture density,  $\varepsilon_f$ .

### 2.7. Estimation of the Horizontal Fracture (HF) Indicator from Elastic Properties

For the characterization of horizontal fractures by using seismic data, it is essential to find an applicable seismic attribute that correlates with the fracture density,  $\varepsilon_f$ , estimated by using the method presented in Figure 3. Based on the framework of the Poisson impedance [53–55], a horizontal fracture (HF) indicator was then proposed, as represented by seismic attributes in Equation (13):

$$\text{HF}(\theta) = I_p \cos \theta - V_p/V_s \sin \theta \quad (13)$$

where  $\theta$  represents the rotation angle that transforms the P-wave impedance ( $I_p$ ) and P-to-S-wave velocity ratio ( $V_p/V_s$ ) to HF.

Then, the maximum correlation between  $\text{HF}(\theta)$  (as represented by Equation (13)) and  $\varepsilon_f$  (as predicted from well-log data) was determined by optimizing the  $\theta_{\text{max}}$  value. By using the seismic-derived elastic properties, the obtained  $\text{HF}(\theta_{\text{max}})$  was, thereafter, used to estimate the horizontal fractures in the shale oil reservoirs.

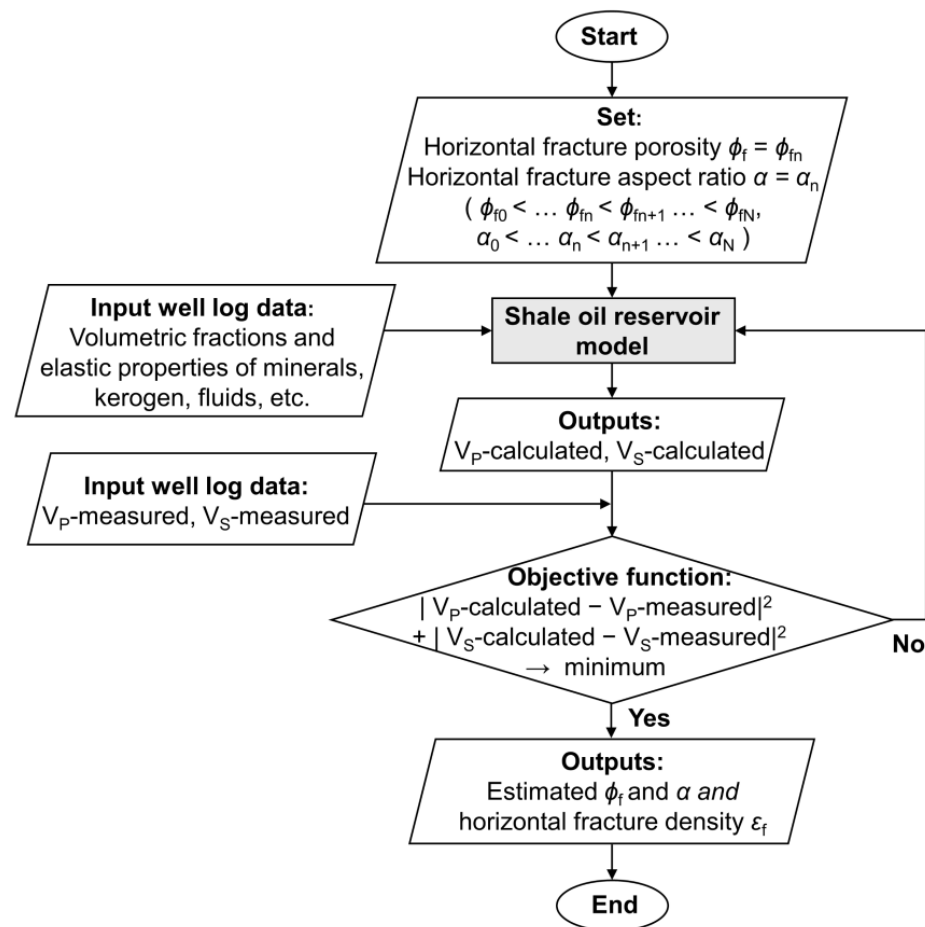


**Figure 3.** Workflow for the prediction of horizontal fractures using the shale model and well-log data.

### 3. Results

#### 3.1. Studied Area and Datasets

As can be seen in Figure 4a, the Nanxiang Basin is located in the middle south of China. Biyang Sag is a secondary structural unit of the Nanxiang Basin, which is located northeast of the Nanxiang Basin (Figure 4b). In the present study, the studied area of the shale oil reservoirs is located in the lower middle of the Biyang Sag, as denoted by the red box in Figure 4b. Also, Figure 5 illustrates the stratigraphic units and sedimentary facies in the studied area. For the studied area, the Taicangfang-Yuhuangding, Hetaoyuan, and Liaozhuang formations have been developed in the Paleogene, while the Shangsi formation has been developed in the Neogene in the studied area. The deposition period of the Hetaoyuan formation in the Biyang Sag overlaps with the peak period of the lacustrine basin development, and the sedimentary facies are characterized by shallow to deep lacustrine facies. The shale is mainly developed in the second (Eh<sub>2</sub>) and third (Eh<sub>3</sub>) members of the Hetaoyuan formation, and the Eh<sub>3</sub> is the main oil-bearing layer in the Biyang Sag. There are six sets of organic material-rich intervals (ORI), as indicated by 1-6 from top to bottom, in the Eh<sub>3</sub>. Out of these, the ORI 5 is a great organic enrichment layer with a large cumulative thickness and a high total organic content. It shows a good shale oil resource potential as the main exploration target reservoir [56,57].

The seismic data were obtained by a three-dimensional seismic acquisition in the studied area. As can be seen in Figure 6, the map of the seismic two-way time for the target shale oil reservoir showed that the geological structure of the target layer was relatively smooth. The positions of the oil wells (A, B, and D) and the dry well (C), as well as the seismic lines across these wells, are illustrated in Figure 6. Among these, wells A, B, and C are vertical wellbores, while well D has a range of horizontal trajectories. Furthermore,

Figure 7 shows the seismic profile where the horizons of the target shale oil layer are indicated. The bottom line in Figure 7 illustrates the bottom limit selected for seismic inversion of elastic parameters and the estimation of HF accordingly. For the studied area, the three-dimensional data volumes of the elastic properties were obtained by a pre-stack seismic inversion.

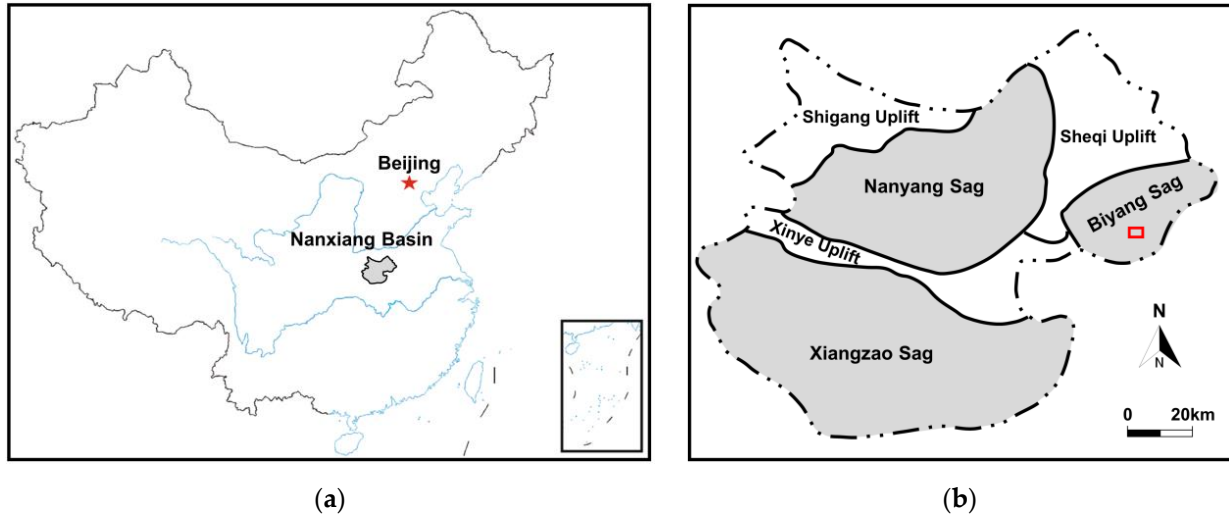


Figure 4. (a) Location of the Nanxiang Basin in China, (b) Location of the Biyang Sag in the Nanxiang Basin, where the red rectangle indicates the studied area in the present investigation.

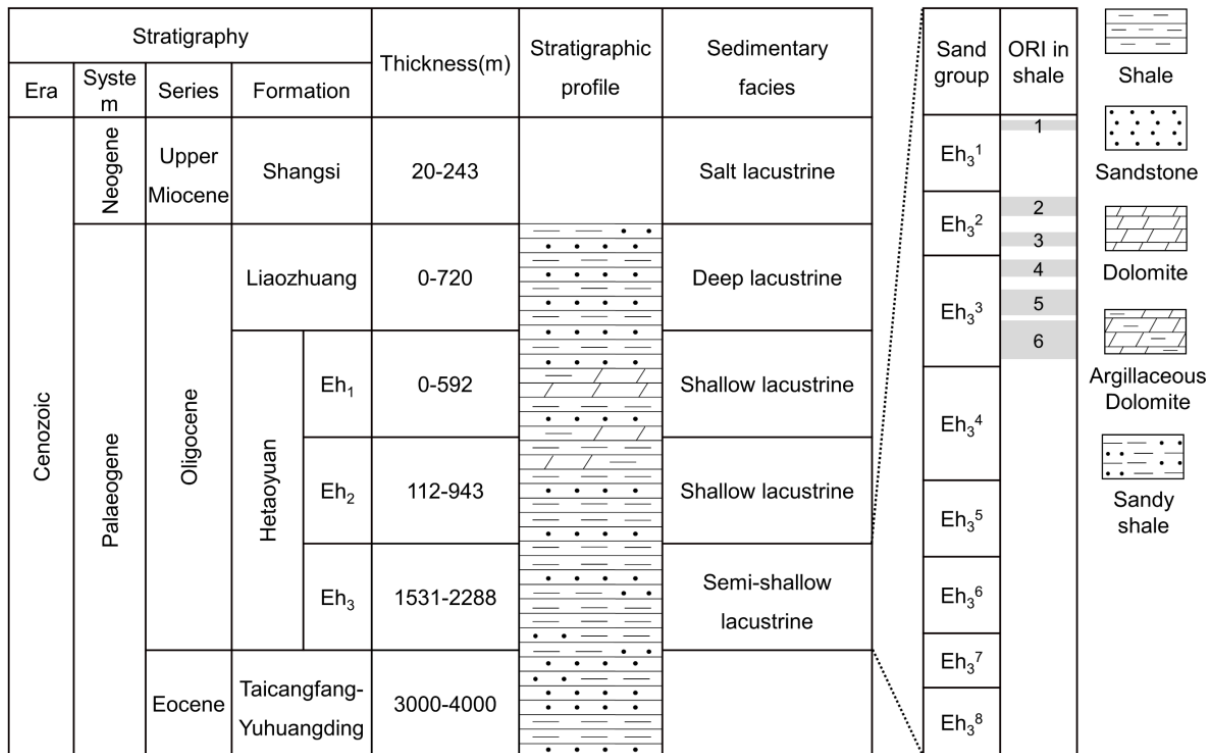
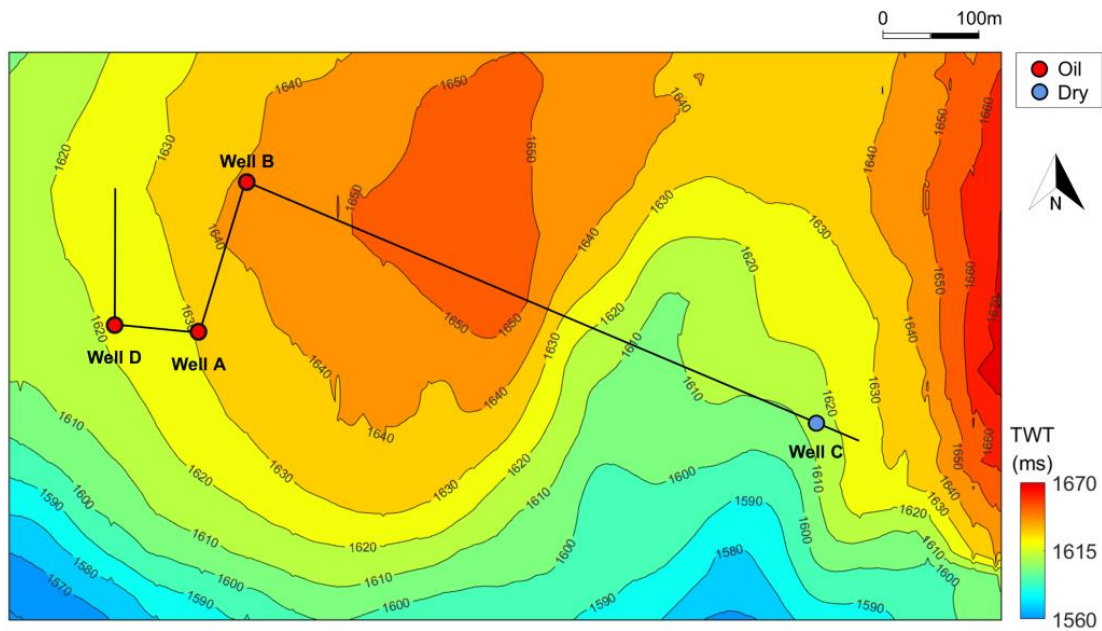
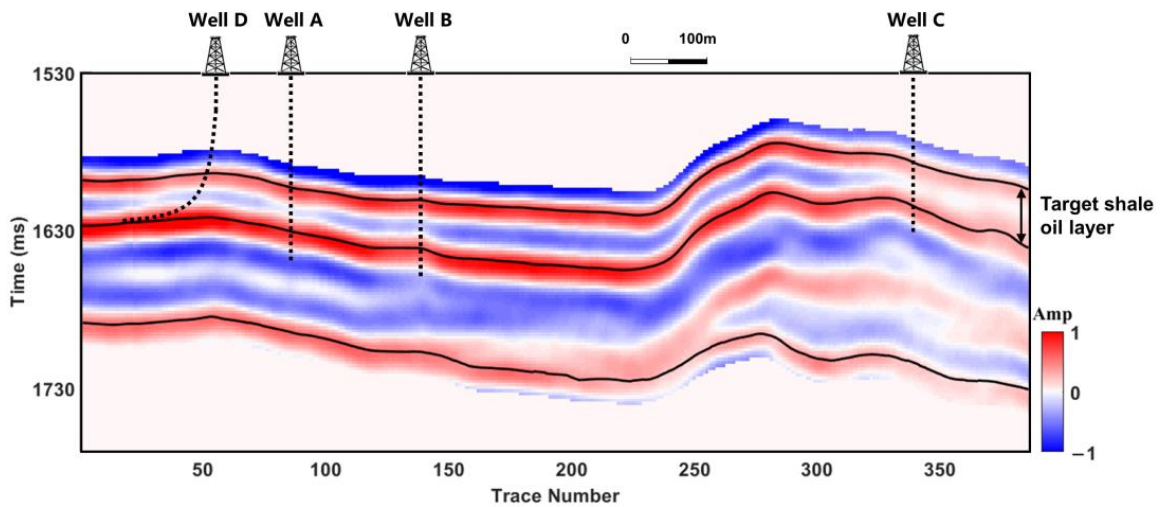


Figure 5. Stratigraphic units and sedimentary facies in the studied area.



**Figure 6.** Two-way time (TWT) for the shale oil reservoir. The red and blue dots indicate the locations of oil and dry wells, respectively. The straight lines denote the seismic lines across the wells.



**Figure 7.** Seismic profile across the wells.

The measured logging curves for well A are displayed in Figure 8, where the interval of the target shale is especially indicated. The target shale layer had a medium porosity ( $\phi$ ) and relatively high oil saturation ( $S_o$ ). According to the geological analyses of the studied region, the horizontal fractures were supposed to contribute to the reservoir permeability and affect the ultimate production. As shown in Figure 9, the formation micro-scanner image (FMI) for well A indicated the presence of horizontal fractures in the target shale layer (as indicated by green and blue lines). It is, therefore, important to estimate the horizontal fractures by using shale modeling and logging data and to predict the horizontal fracture distributions by using seismic-inverted elastic properties. Accordingly, rock physical modeling has been performed based on the logging data from well A. The horizontal fractures were then estimated, followed by the establishment of a correlation between the horizontal fractures and elastic properties.

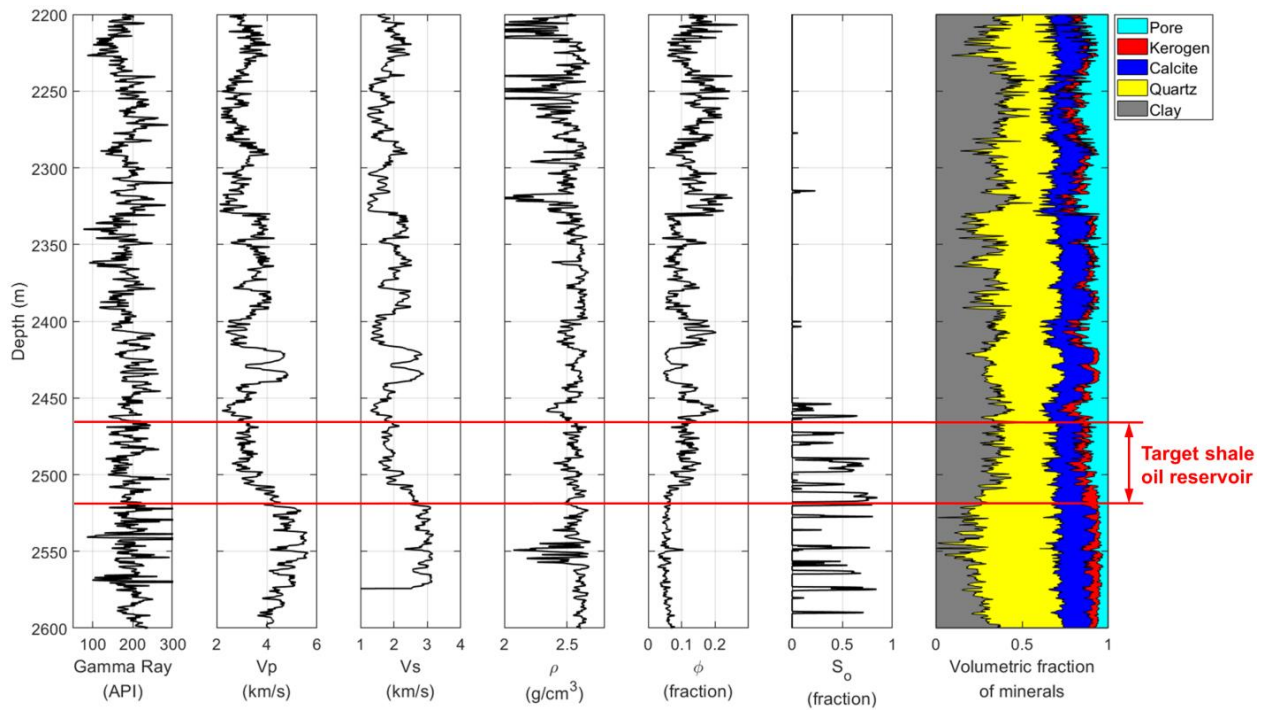


**Figure 8.** Logging curves from well A, including the gamma-ray (GR) values, P-wave velocity ( $V_P$ ), S-wave velocity ( $V_S$ ), density ( $\rho$ ), porosity ( $\phi$ ), oil saturation ( $S_o$ ), and volumetric fraction of minerals.

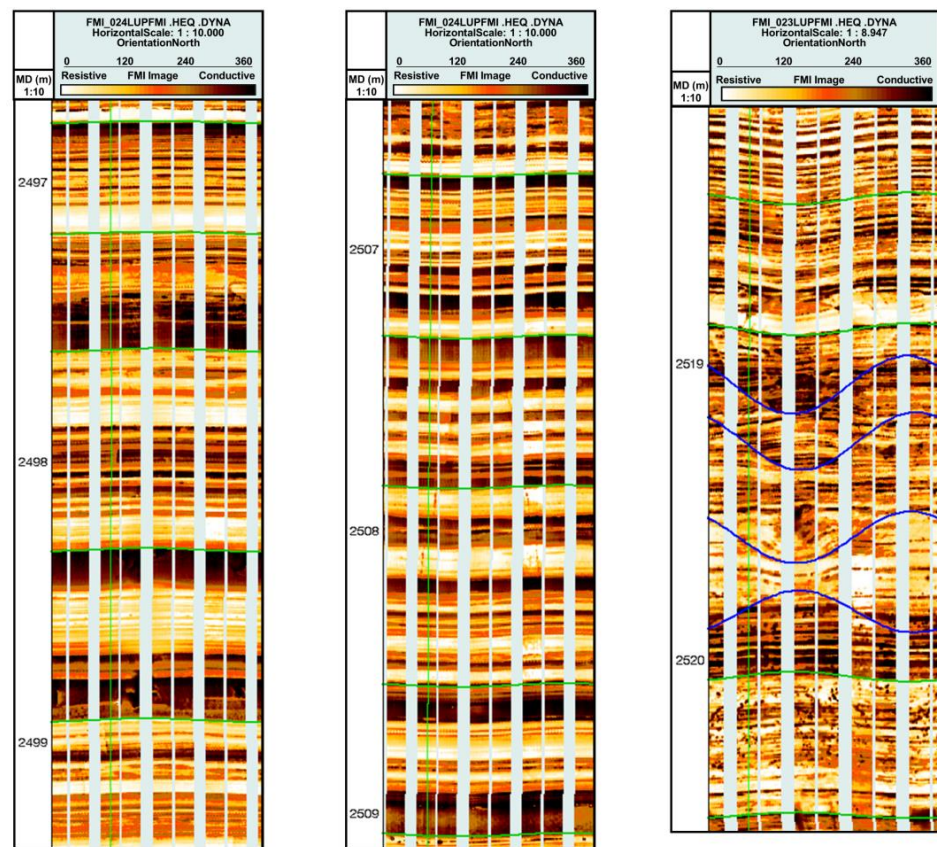


**Figure 9.** Formation micro-scanner image (FMI) for the target shale layer in well A.

### 3.2. Prediction of the Horizontal Fracture Density by Using the Shale Model and Logging Data

Based on the shale model (see Figure 2) and the modeling framework (see Figure 3), the horizontal fracture porosity,  $\phi_f$ , and the corresponding aspect ratio,  $\alpha$ , have been calculated using logging data illustrated in Figure 8, with the obtained results presented in Figure 10. Table 1 presents the elastic properties of the components that were used in the modeling. The logarithmic value of the aspect ratio ( $\log(\alpha)$ ) of the horizontal fracture was then used for simplicity. In Figure 10, the modeled  $V_P$  and  $V_S$  according to Equations (14) and (15):

$$V_P = \sqrt{\frac{c_{33}}{\rho}}, V_S = \sqrt{\frac{c_{44}}{\rho}} \quad (14)$$

$$\rho = (1 - \phi) \sum_{i=1}^n f_i \rho_i + \phi \rho_f \quad (15)$$

where  $\rho$  represents the rock density,  $\phi$  is the total porosity, and  $\rho_f$  is calculated using Equation (11).  $f_1$  and  $\rho_i$  are the volume fraction and density of each component, respectively. Elastic stiffnesses  $c_{33}$  and  $c_{44}$  are calculated using the Hudson model illustrated in Section 2.4.

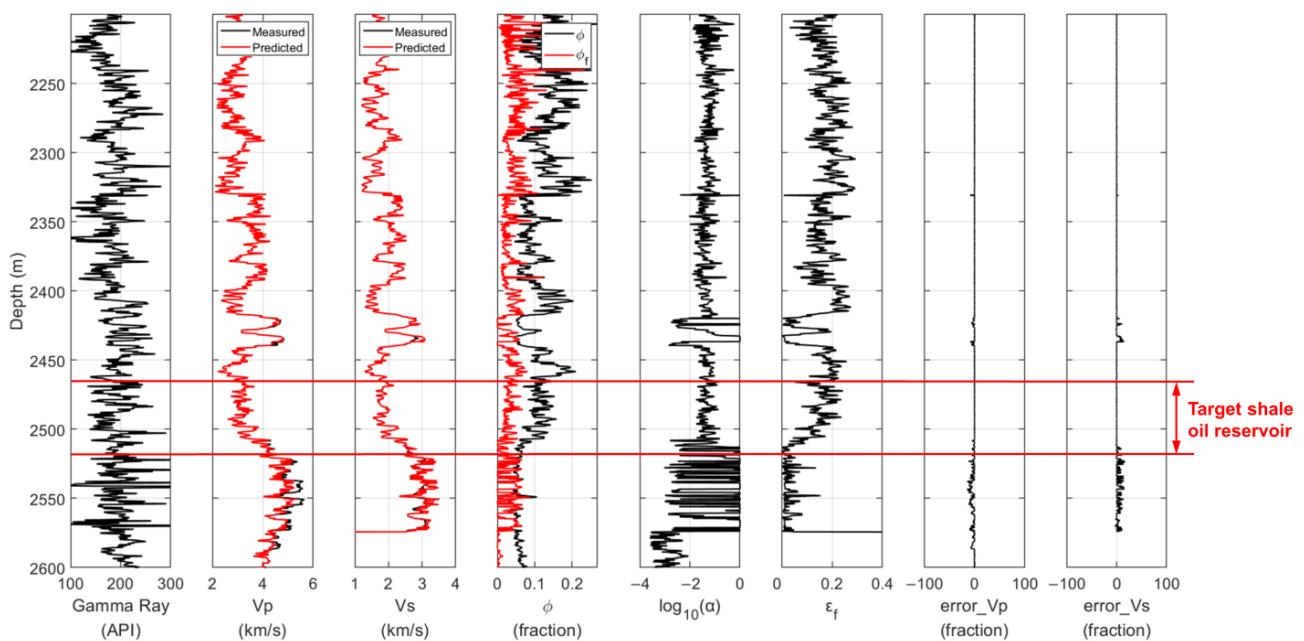


**Figure 10.** Logging curves and rock physical modeling results for well A, including curves of the gamma-ray (GR) value, P-wave velocity ( $V_P$ ), S-wave velocity ( $V_S$ ), porosity ( $\phi$ ), logarithm value of the horizontal fracture aspect ratio ( $\log(\alpha)$ ), fracture density ( $\epsilon_f$ ), relative error of  $V_P$  (error\_  $V_P$ ), and relative error of  $V_S$  (error\_  $V_S$ ).

**Table 1.** Properties of the components that have been used for the modeling [58].

	Clay	Quartz	Calcite	Kerogen	Oil	Water
$V_P$ (km/s)	3.6	6.05	6.84	2.6	0.9	1.47
$V_S$ (km/s)	1.85	4.36	3.72	1.5	0	0
$\rho$ (g/cm <sup>3</sup> )	2.58	2.65	2.75	1.35	0.7	1.04

As can be seen in Figure 10, the modeled  $V_P$  and  $V_S$  (red curves) were obtained using the fitting parameters  $\phi_f$  and  $\alpha$ . They clearly agree with the corresponding measured values (black curves), thereby validating the applicability of the modeling method. The predicted

$\phi_f$  value shows how much pore space was occupied by horizontal fractures in the total porosity. In addition, the estimated  $\alpha$  value shows the geometry of the horizontal fractures. According to Equation (7), it could be used to obtain the fracture density ( $\varepsilon_f$ ), thereby providing a comprehensive evaluation of the horizontal fracture properties.

### 3.3. Obtaining the HF Indicator for the Horizontal Fracture Estimation of Shale Oil Reservoirs

Based on the results from the rock physical modeling (Figure 10), the HF indicator has been further evaluated according to Equation (13) for the evaluation of horizontal fractures in the shale oil reservoirs. As color-coded by  $\varepsilon_f$  in Figure 11, the cross-plots of  $I_P$  and the  $V_P/V_S$  ratio have been obtained by using the results presented in Figure 10. The separable distributions of data clusters in the cross-plots showed the possibility for a determination of  $\varepsilon_f$  values from the elastic properties. Furthermore, the optimal rotation angle ( $\theta_{max}$ ) in Equation (13) has been determined by using the framework of the Poisson impedance. As illustrated in Figure 12, a maximum correlation coefficient was found between  $\varepsilon_f$  and HF represented by elastic properties ( $I_P$  and  $V_P/V_S$ ) at  $\theta_{max} = 83^\circ$ . Accordingly, the obtained HF indicator shows a good correlation with  $\varepsilon_f$  (Figure 13). Higher values of HF corresponded to an increase in  $\varepsilon_f$ , implying that the obtained HF acts as an effective indicator in the evaluation of the development of horizontal fractures in the shale. However, it must be stressed that since HF was obtained from the combination of  $I_P$  and  $V_P/V_S$ , the values of HF in Figure 13 had no actual physical meaning.

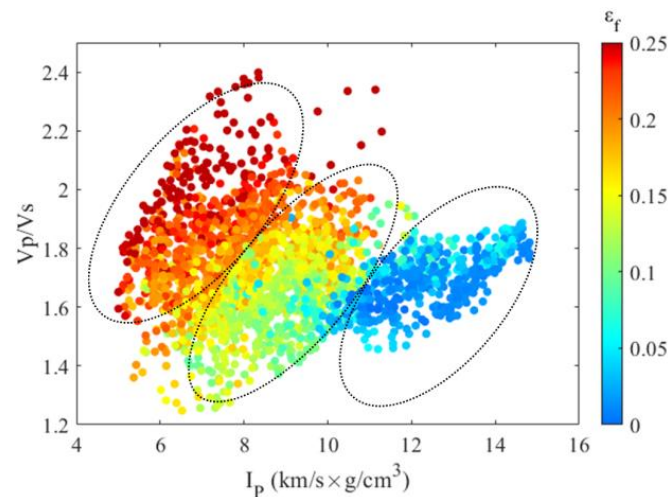


Figure 11. Cross-plot of  $I_P$  and  $V_P/V_S$ , as color-coded by  $\varepsilon_f$ .

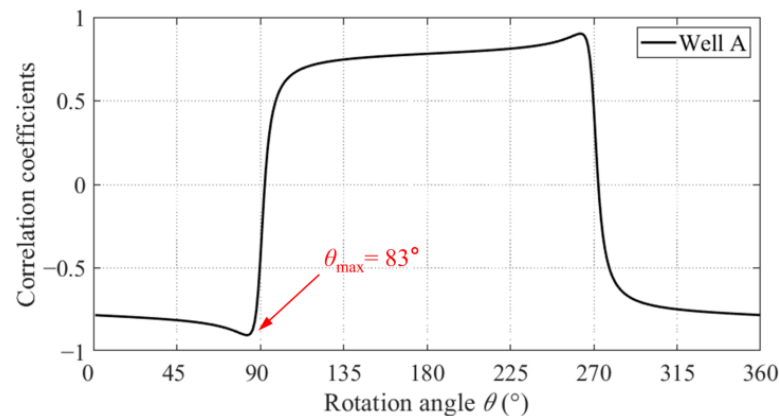
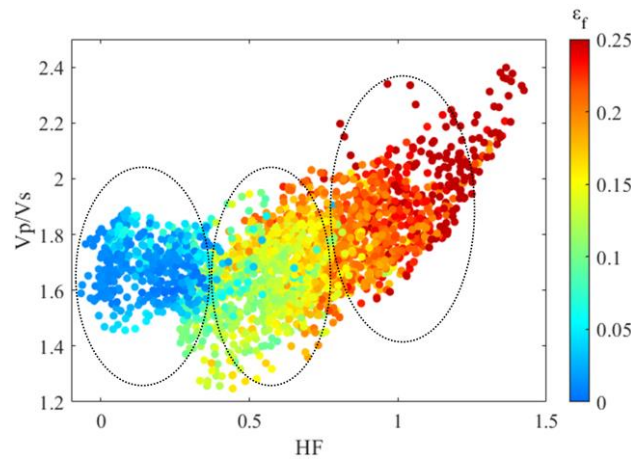


Figure 12. Correlation coefficient variations with the rotation angle,  $\theta$ .



**Figure 13.** Cross-plot of HF ( $\theta_{\max} = 83^\circ$ ) and  $V_p/V_s$ , as color-coded by  $\epsilon_f$ .

3.4. Estimations of HF and TOC by Using Seismic Data

The obtained HF was further used for seismic data for a quantitative interpretation of the horizontal fractures. Figures 14 and 15 illustrate the cross-well seismic profiles of  $I_p$  and  $V_p/V_s$ , respectively. The HF factor, calculated from Figures 14 and 15, was presented in Figure 16. To avoid any confusion, it should be noted that the HF factor in Figure 16 has been labeled using high and low magnitudes. The reason is that the HF value had no actual physical meaning, which has also been mentioned above in association with Figure 13.

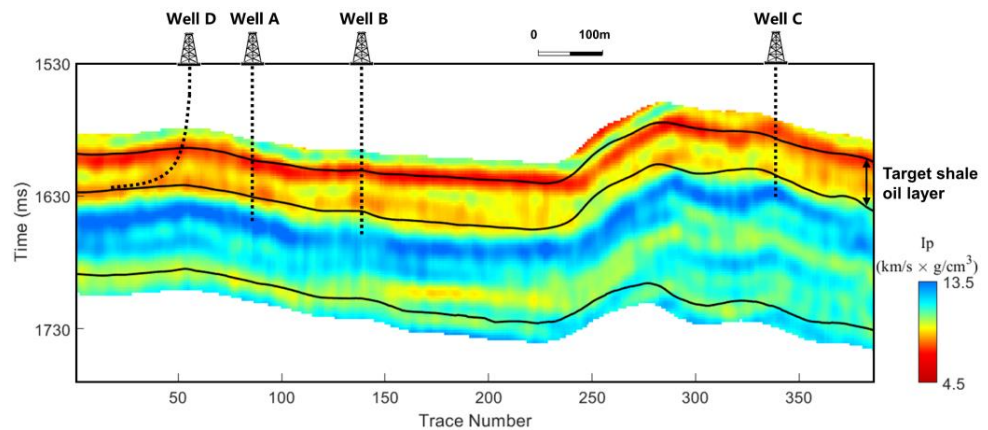


**Figure 14.** Profile of the  $I_p$  crossing wells.

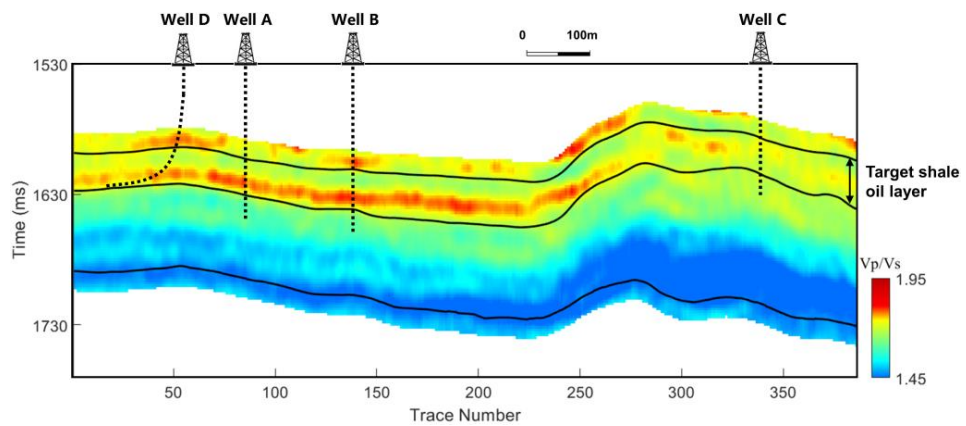


**Figure 15.** Profile of the  $V_p/V_s$  crossing wells.

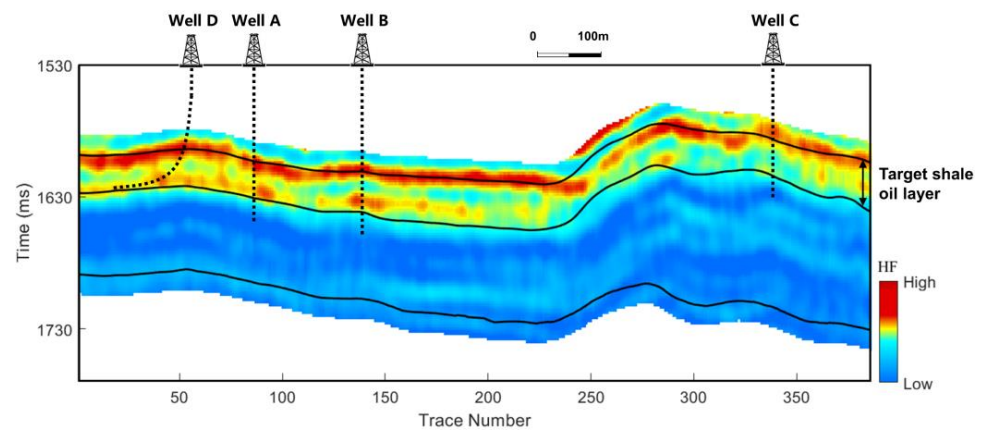


**Figure 16.** Profile of the HF crossing wells.

As was discussed above, the obtained HF factor could be used as an effective indicator in the prediction of the development of horizontal fractures in shale oil reservoirs. The results presented in Figure 16 indicate that the target shale oil layer showed relatively large HF anomalies in the oil-producing wells A, B, and D, while exhibiting no anomalies in the dry well C. This consistency showed the importance of horizontal fractures for the ultimate productivity of shale oil reservoirs.

To further evaluate the importance of horizontal fractures for the ultimate oil productivity, the TOC of the shale oil reservoirs has been calculated based on the regression analysis of TOC versus density ( $\rho$ ) by using logging data from well A (Figure 17). Subsequently, the TOC section (Figure 18) was derived from the seismic-inverted  $\rho$  based on the obtained linear regression presented in Figure 17. As can be seen in Figure 18, the target shale oil reservoir shows high TOC values for all oil wells (A, B, and D), and a relatively high TOC value for the dry well C. By comparing Figures 16 and 18, the results indicate that the shale with the high TOC value, but a low horizontal fracture density (i.e., in well C), produces no oil. This shows that horizontal fractures are essential for the prediction of high-quality shale oil reservoirs.

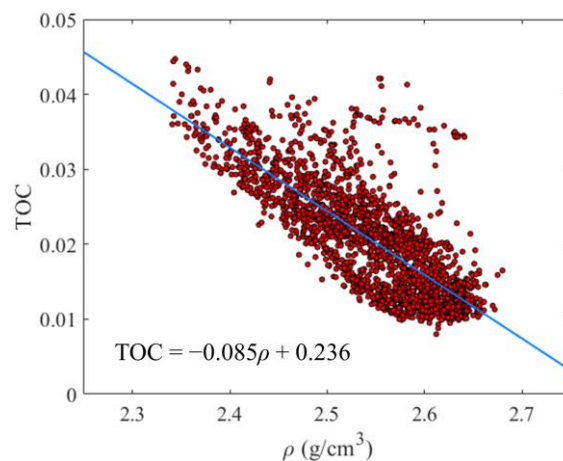


**Figure 17.** Linear regression of TOC versus  $\rho$ , using logging data from well A.

Finally, the  $I_P$  and  $V_P/V_S$  maps for the target shale oil reservoir are displayed in Figures 19 and 20, respectively. Accordingly, the computed map of HF (Figure 21) is of great help for the comprehensive characterization of the shale oil reservoirs with simultaneous consideration of the TOC (Figure 22) derived from the seismic-inverted  $\rho$ .

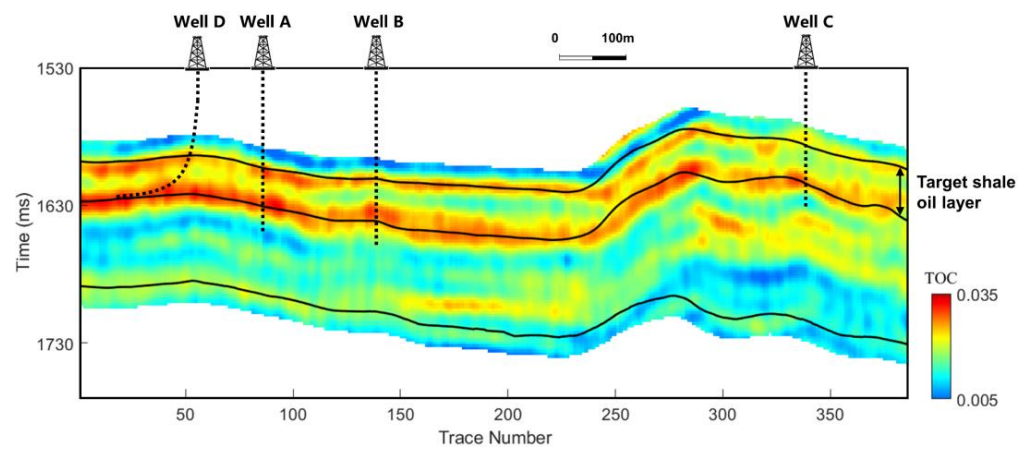


Figure 18. Profile of the TOC crossing wells.

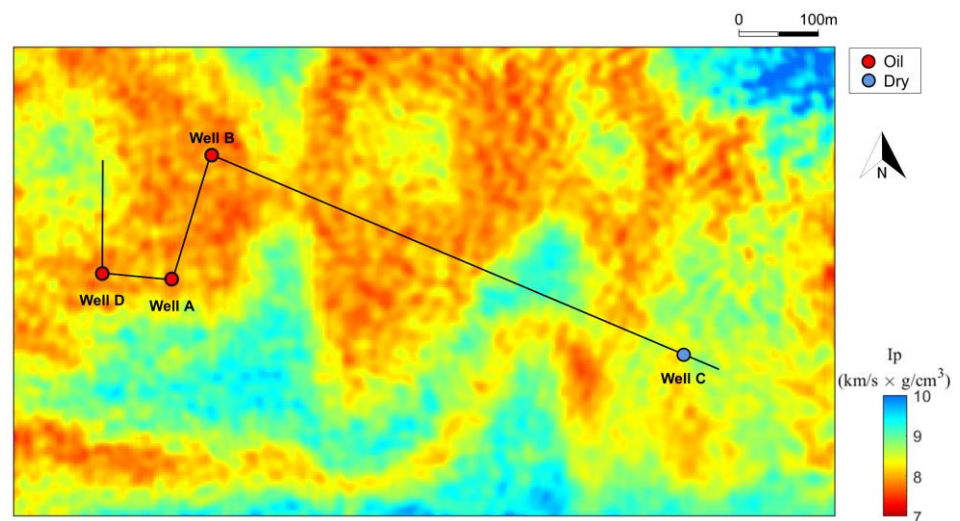


Figure 19. Horizontal map of  $I_p$  for the target shale.

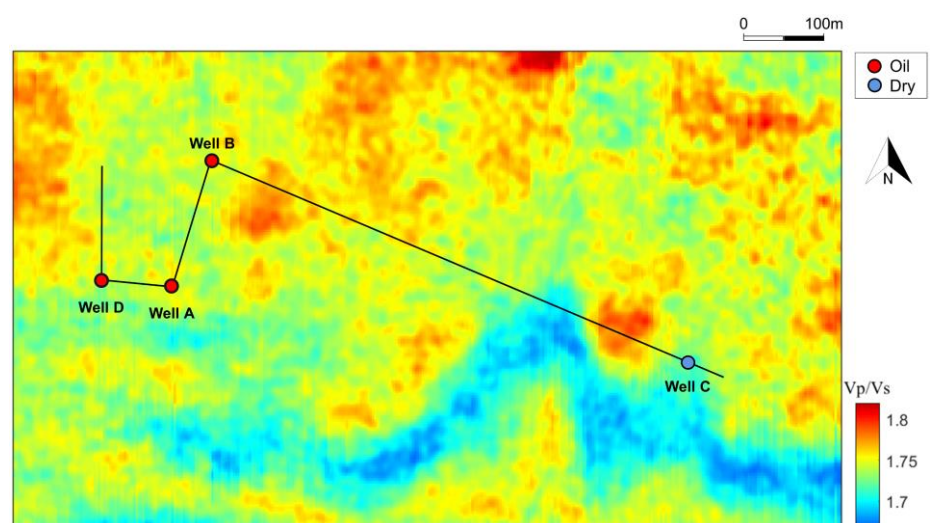


Figure 20. Horizontal map of  $V_p/V_s$  for the target shale.

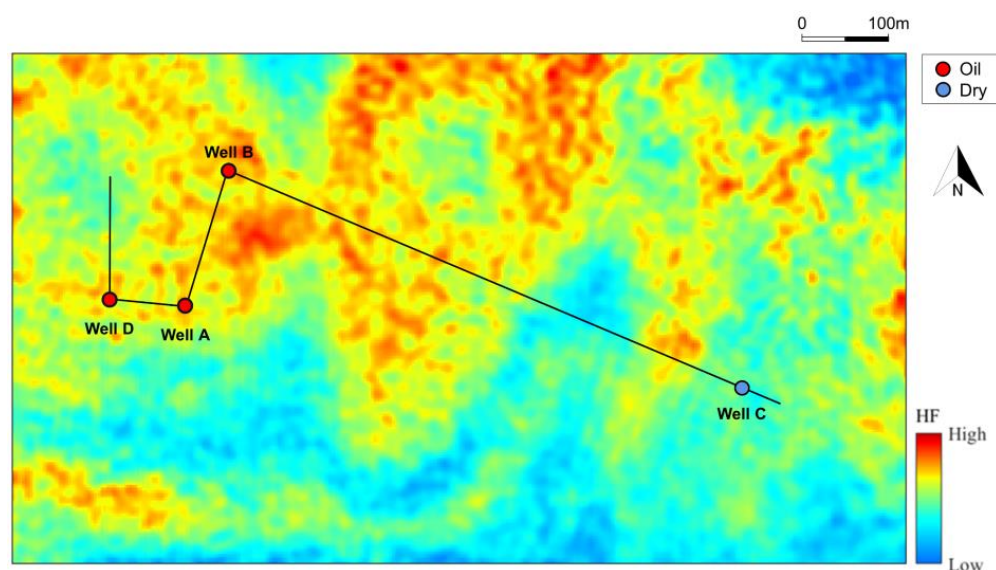


Figure 21. Horizontal map of HF for the target shale.

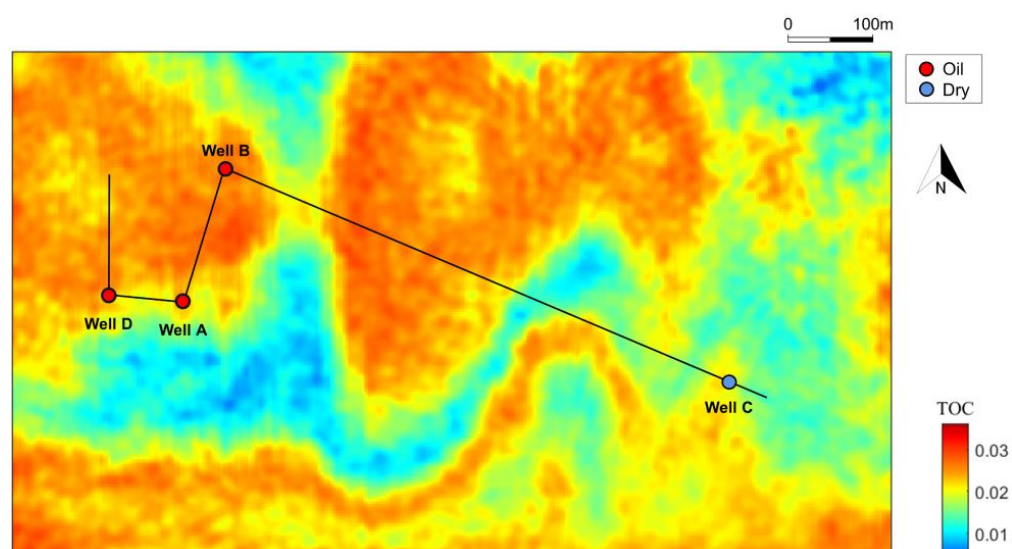


Figure 22. Horizontal map of TOC for the target shale.

#### 4. Discussion

Numerous shale models have been proposed that relate the microstructures with the elastic properties of shale rocks. To achieve the objectives in the present study, appropriate modeling methods have been proposed to successfully predict horizontal fractures in the shales (Figures 1 and 2). The main purpose of the proposed shale model was to quantify the elastic properties of the shale that has a total pore space occupied by matrix pores and horizontal fractures. In the modeling based on the shale model and logging data, horizontal fracture properties,  $\phi_f$  and  $\alpha$ , were estimated by using a rock physical inversion scheme (Figure 3). The obtained results were further used to derive the  $\varepsilon_f$  values for a comprehensive representation of the horizontal fractures (Figure 10). The modeling results showed that the modeled  $V_P$  and  $V_S$  fitted quite well with the measured  $V_P$  and  $V_S$  curves, which validated the applicability of the proposed shale model and the rationality of the calculated horizontal fracture properties ( $\phi_f$ ,  $\alpha$ , and  $\varepsilon_f$ ).

The separable distribution of data clusters in the cross-plot of  $I_P$  and the  $V_P/V_S$  ratio showed that it is possible to determine  $\varepsilon_f$  using elastic properties (Figure 11). Accordingly, by using the framework of the Poisson impedance, the HF indicator was further proposed

to estimate  $\varepsilon_f$  in terms of elastic properties (Equation (13)). With the calculated optimal rotation angle, the obtained HF factor showed a good correlation with  $\varepsilon_f$ . This result highlighted the effectiveness of HF in the evaluation of horizontal fractures in shale oil reservoirs (Figures 12 and 13).

The obtained HF factor was further applied to seismic data for a quantitative interpretation of the horizontal fractures. The results showed that the shale oil reservoir had relatively high HF anomalies in the oil-producing wells A, B, and D, while exhibiting no anomalies in the dry well C (Figure 16). This regularity emphasized the importance of horizontal fractures for the ultimate productivity of the shale oil reservoirs.

The TOC section was further estimated by performing a regression analysis of TOC versus  $\rho$ . The effect of horizontal fractures on the ultimate oil productivity was thereby further evaluated. Also, a comparison of HF and TOC (Figures 16 and 18, respectively) indicated that the shale with a high TOC value, but with a low horizontal fracture density, produced no oil. The results indicated that the horizontal fractures were important in the prediction of high-quality shale oil reservoirs. Nevertheless, other factors (including the TOC, brittleness of the reservoir, and hydraulic fracturing performance) should be considered for an effective evaluation of the shale oil reservoirs.

## 5. Conclusions

A framework that predicts horizontal fractures in shale oil reservoirs has been developed in the present study. A shale model was used as a rock physical modeling tool with logging data as input. An effective indicator for the evaluation of horizontal fractures was established by using the modeling results. The proposed indicator was then applied to seismic data for a quantitative interpretation of horizontal fractures in shale oil reservoirs by using seismic-inverted elastic properties. The main conclusions from this investigation were as follows:

- (1) The proposed shale model was capable of quantifying the elastic responses of shale oil reservoirs that were associated with horizontal fracture properties. This result was validated by modeling results based on logging data. In the modeling, the calculated  $V_P$  and  $V_S$  showed a good agreement with the corresponding measured values. In addition, the predicted fracture properties,  $\phi_f$  and  $\alpha$ , were used to obtain the fracture density,  $\varepsilon_f$ , for further evaluation of horizontal fractures.
- (2) According to the framework of the Poisson impedance, the HF indicator was proposed to represent  $\varepsilon_f$  in terms of a combination of elastic properties ( $I_P$  and  $V_P/V_S$ ). This enabled a quantitative interpretation of the development of horizontal fractures by using seismic-inverted elastic properties. Also, the established HF indicator showed a good correlation with  $\varepsilon_f$ . The increasing HF indicated an increase in  $\varepsilon_f$ , which showed that the proposed HF factor was an effective indicator in the prediction of horizontal fractures in shale oil reservoirs.
- (3) The seismic data applications showed that the target shale oil layer had high HF anomalies in the oil-producing wells, while exhibiting no anomalous response in the dry well. The consistency between the development of horizontal fractures and the production status of the boreholes highlighted the importance of horizontal fractures for the ultimate productivity of shale oil reservoirs. This result indicated that the horizontal fractures were essential in the prediction of high-quality shale oil reservoirs.

In future studies, the advancement of experiments and modeling methods can provide further insights into the effects of horizontal fractures on the seismic signatures of shale oil reservoirs. Based on these developments, other effective shale models, with corresponding parameters, can be developed for improved characterization of horizontal fractures in shale oil reservoirs.

**Author Contributions:** Conceptualization, Z.G.; methodology, Z.G.; software, W.G.; validation, Z.G. and W.G.; formal analysis, Z.G.; investigation, Z.G., W.G. and C.L.; resources, C.L.; data curation, W.G.; writing—original draft preparation, Z.G. and W.G.; writing—review and editing, Z.G.; visualization, W.G.; project administration, Z.G.; funding acquisition, Z.G. All authors have read and agreed to the published version of the manuscript.

**Funding:** This research was funded by the National Natural Science Foundation of China, grant numbers 42274160 and 42074153.

**Data Availability Statement:** Data are contained within the article.

**Conflicts of Interest:** The authors declare no conflict of interest.

## References

1. Xu, C.Y.; Zhu, L.M.; Xu, F.; Kang, Y.L.; Jing, H.R.; You, Z.J. Experimental study on the mechanical controlling factors of fracture plugging strength for lost circulation control in shale gas reservoir. *Geoen. Sci. Eng.* **2023**, *231*, 212285. [[CrossRef](#)]
2. Diwu, P.X.; Liu, T.J.; You, Z.J.; Jiang, B.Y.; Zhou, J. Effect of low velocity non-Darcy flow on pressure response in shale and tight oil reservoirs. *Fuel* **2018**, *216*, 398–406. [[CrossRef](#)]
3. Feng, G.J.; Zhu, Y.M.; Chen, S.B.; Wang, Y.; Ju, W.; Hu, Y.C.; You, Z.J.; Wang, G.G. Supercritical methane adsorption on shale over wide pressure and temperature ranges: Implications for gas-in-place estimation. *Energy Fuel.* **2020**, *34*, 3121–3134. [[CrossRef](#)]
4. Xu, C.Y.; Kang, Y.L.; You, Z.J.; Chen, M.J. Review on formation damage mechanisms and processes in shale gas reservoir: Known and to be known. *J. Nat. Gas Sci. Eng.* **2016**, *36*, 1208–1219. [[CrossRef](#)]
5. Vernik, L.; Milovac, J. Rock physics of organic shales. *Lead. Edge* **2011**, *30*, 318–323. [[CrossRef](#)]
6. Zhao, L.X.; Qin, X.; Zhang, J.Q.; Liu, X.W.; Han, D.H.; Geng, J.H.; Xiong, Y.N. An Effective Reservoir Parameter for Seismic Characterization of Organic Shale Reservoir. *Surv. Geophys.* **2018**, *39*, 509–541. [[CrossRef](#)]
7. Deng, X.H.; Liu, C.; Guo, Z.Q.; Liu, X.W.; Liu, Y.W. Rock physical inversion and quantitative seismic interpretation for the Longmaxi shale gas reservoir. *J. Geophys. Eng.* **2019**, *16*, 652–665. [[CrossRef](#)]
8. Yin, L.J.; Yin, X.Y.; Zong, Z.Y.; Chen, B.C.; Chen, Z.Q. A new rock physics model method for shale on the theory of micro-nanopores. *Chin. J. Geophys.* **2020**, *63*, 1642–1653. [[CrossRef](#)]
9. Guo, Z.Q.; Lv, X.Y.; Liu, C.; Liu, X.W.; Liu, Y.W. Shale gas characterisation for hydrocarbon accumulation and brittleness by integrating a rock-physics-based framework with effective reservoir parameters. *J. Nat. Gas Sci. Eng.* **2022**, *100*, 104498. [[CrossRef](#)]
10. Goodway, B.; Varsek, J.; Abaco, C. Isotropic AVO methods to detect fracture prone zones in tight gas resource plays. In *CSPG CSEG Convention; CSPG CSEG: Calgary, AB, Canada*, 2007.
11. Rickman, R.; Mullen, M.; Petre, E. A practical use of shale petrophysics for stimulation design optimization: All shale plays are not clones of the Barnett Shale. In *Proceedings of the SPE Annual Technical Conference and Exhibition, Denver, CO, USA*, 21–24 September 2008; SPE: Denver, CO, USA, 2008.
12. Waters, G.A.; Lewis, R.E.; Bentley, D.C. The effect of mechanical properties anisotropy in the generation of hydraulic fractures in organic shales. In *Proceedings of the SPE Middle East Unconventional Gas Conference and Exhibition, Denver, CO, USA*, 30 October–2 November 2011; SPE: Abu Dhabi, United Arab Emirates, 2011.
13. Slatt, R.M.; Abousleiman, Y. Merging sequence stratigraphy and geomechanics for unconventional gas shales. *Lead. Edge* **2011**, *30*, 274–282. [[CrossRef](#)]
14. Guo, Z.Q.; Li, X.Y.; Liu, C.; Feng, X.; Shen, Y. A shale rock physics model for analysis of brittleness index, mineralogy and porosity in the Barnett Shale. *J. Geophys. Eng.* **2013**, *10*, 025006. [[CrossRef](#)]
15. Chen, J.J.; Zhang, G.Z.; Chen, H.Z.; Yin, X.Y. The Construction of Shale Rock Physics Effective Model and Prediction of Rock Brittleness. In *Proceedings of the SEG Annual Meeting, Denver, CO, USA*, 26–31 October 2014; SEG: Denver, Colorado, USA, 2014.
16. Bachrach, R.; Sengupta, M.; Salama, A.; Miller, P. Reconstruction of the layer anisotropic elastic parameters and high-resolution fracture characterization from P-wave data: A case study using seismic inversion and Bayesian rock physics parameter estimation. *Geophys. Prospect.* **2009**, *57*, 253–262. [[CrossRef](#)]
17. Far, M.E.; Thomsen, L.; Sayers, C.M. Inversion for asymmetric fracture parameters using synthetic AVOA data. In *Society of Exploration Geophysicists International Exposition; SEG: Las Vegas, NV, USA*, 2012.
18. Zhang, G.Z.; Chen, H.Z.; Yin, X.Y.; Li, N.; Yang, B.J. Method of Fracture Elastic Parameter Inversion Based on Anisotropic AVO. *J. Jilin Univ. (Earth Sci. Ed.)* **2012**, *42*, 845–851, 871. [[CrossRef](#)]
19. Chen, H.Z.; Yin, X.Y.; Gao, C.G.; Zhang, G.Z.; Chen, J.J. AVAZ inversion for fluid factor based on fracture anisotropic rock physics theory. *Chin. J. Geophys.* **2014**, *57*, 968–978. [[CrossRef](#)]
20. Chen, H.Z.; Zhang, G.Z.; Ji, Y.X.; Yin, X.Y. Azimuthal seismic amplitude difference inversion for fracture weakness. *Pure Appl. Geophys.* **2017**, *174*, 279–291. [[CrossRef](#)]
21. Pan, X.; Zhang, G. Fracture detection and fluid identification based on anisotropic Gassmann equation and linear-slip model. *Geophysics* **2019**, *84*, R99–R112. [[CrossRef](#)]

22. Luo, T.; Feng, X.; Guo, Z.; Liu, C.; Liu, X.W. Seismic AVAZ inversion for orthorhombic shale reservoirs in the Longmaxi area, Sichuan. *Appl. Geophys.* **2019**, *16*, 185–198. [[CrossRef](#)]
23. Pan, X.P.; Zhang, P.F.; Zhang, G.Z.; Guo, Z.W.; Liu, J.X. Seismic characterization of fractured reservoirs with elastic impedance difference versus angle and azimuth: A low-frequency poroelasticity perspective. *Geophysics* **2021**, *86*, M123–M139. [[CrossRef](#)]
24. Vernik, L.; Nur, A. Ultrasonic velocity and anisotropy of hydrocarbon source rocks. *Geophysics* **1992**, *57*, 727–735. [[CrossRef](#)]
25. Vernik, L.; Landis, C. Elastic anisotropy of source rocks: Implications for hydrocarbon generation and primary migration. *AAPG Bull.* **1996**, *80*, 531–544. [[CrossRef](#)]
26. Carcione, J.M. A model for seismic velocity and attenuation in petroleum source rocks. *Geophysics* **2000**, *65*, 1080–1092. [[CrossRef](#)]
27. Carcione, J.M. AVO effects of a hydrocarbon source-rock layer. *Geophysics* **2001**, *66*, 419–427. [[CrossRef](#)]
28. Carcione, J.M.; Helle, H.B.; Avseth, P. Source-rock seismic-velocity models: Gassmann versus Backus. *Geophysics* **2011**, *76*, N37–N45. [[CrossRef](#)]
29. Sayers, C.M. The effect of kerogen on the AVO response of organic-rich shales. *Lead. Edge* **2013**, *32*, 1514–1519. [[CrossRef](#)]
30. Sayers, C.M.; Guo, S.; Silva, J. Sensitivity of the elastic anisotropy and seismic reflection amplitude of the Eagle Ford Shale to the presence of kerogen. *Geophys. Prospect.* **2015**, *63*, 151–165. [[CrossRef](#)]
31. Vernik, L. Hydrocarbon-generation-induced microcracking of source rocks. *Geophysics* **1994**, *59*, 555–563. [[CrossRef](#)]
32. Vernik, L.; Liu, X. Velocity anisotropy in shales: A petrophysical study. *Geophysics* **1997**, *62*, 521–532. [[CrossRef](#)]
33. Liu, J.; Ning, J.R.; Liu, X.W.; Liu, C.Y.; Chen, T.S. An improved scheme of frequency-dependent AVO inversion method and its application for tight gas reservoirs. *Geofluids* **2019**, *2019*, 3525818. [[CrossRef](#)]
34. Zhang, X.M.; Shi, W.Z.; Hu, Q.H.; Zhai, G.Y.; Wang, R.; Xu, X.F.; Meng, F.L.; Liu, Y.Z.; Bai, L.H. Developmental characteristics and controlling factors of natural fractures in the lower paleozoic marine shales of the upper Yangtze Platform, southern China. *J. Nat. Gas Sci. Eng.* **2020**, *76*, 103191. [[CrossRef](#)]
35. Xu, X.; Zeng, L.B.; Tian, H.; Ling, K.G.; Che, S.Q.; Yu, X.; Shu, Z.G.; Dong, S.Q. Controlling factors of lamellation fractures in marine shales: A case study of the Fuling Area in Eastern Sichuan Basin, China. *J. Petrol. Sci. Eng.* **2021**, *207*, 109091. [[CrossRef](#)]
36. He, Z.L.; Li, S.J.; Nie, H.K.; Yuan, Y.S.; Wang, H. The shale gas “sweet window”: “The cracked and unbroken” state of shale and its depth range. *Mar. Petrol. Geol.* **2019**, *101*, 334–342. [[CrossRef](#)]
37. Lu, Y.; Yang, F.; Bai, T.; Han, B.; Lu, Y.; Gao, H. Shale Oil Occurrence Mechanisms: A Comprehensive Review of the Occurrence State, Occurrence Space, and Movability of Shale Oil. *Energies* **2022**, *15*, 9485. [[CrossRef](#)]
38. Gou, Q.; Xu, S. The Controls of Laminae on Lacustrine Shale Oil Content in China: A Review from Generation, Retention, and Storage. *Energies* **2023**, *16*, 1987. [[CrossRef](#)]
39. Xu, S.; Gou, Q. The Importance of Laminae for China Lacustrine Shale Oil Enrichment: A Review. *Energies* **2023**, *16*, 1661. [[CrossRef](#)]
40. Guo, Z.Q.; Liu, C.; Liu, X.W.; Dong, N.; Liu, Y.W. Research on anisotropy of shale oil reservoir based on rock physics model. *Appl. Geophys.* **2016**, *13*, 382–392. [[CrossRef](#)]
41. Guo, Z.Q.; Zhang, X.D.; Liu, C.; Liu, X.W.; Liu, Y.W. Hydrocarbon identification and bedding fracture detection in shale gas reservoirs based on a novel seismic dispersion attribute inversion method. *Surv. Geophys.* **2022**, *43*, 1793–1816. [[CrossRef](#)]
42. Zhao, L.X.; Qin, X.; Han, D.H.; Geng, J.H.; Yang, Z.F.; Cao, H. Rock-physics modeling for the elastic properties of organic shale at different maturity stages. *Geophysics* **2016**, *81*, 527–541. [[CrossRef](#)]
43. Liu, X.W.; Guo, Z.Q.; Liu, C.; Liu, Y.W. Anisotropy rock physics model for the Longmaxi shale gas reservoir, Sichuan Basin, China. *Appl. Geophys.* **2017**, *14*, 21–30. [[CrossRef](#)]
44. Guo, Z.Q.; Lv, X.Y.; Liu, C. Estimating Organic Enrichment in Shale Gas Reservoirs Using Elastic Impedance Inversion Based on an Organic Matter–Matrix Decoupling Method. *Surv. Geophys.* **2023**, *44*, 1985–2009. [[CrossRef](#)]
45. Yi, S.; Pan, S.; Zuo, H.; Wu, Y.; Song, G.; Gou, Q. Research on Rock Physics Modeling Methods for Fractured Shale Reservoirs. *Energies* **2023**, *16*, 226. [[CrossRef](#)]
46. Guo, Z.Q.; Li, X.Y.; Liu, C. Anisotropy parameters estimate and rock physics analysis for the Barnett Shale. *J. Geophys. Eng.* **2014**, *11*, 065006. [[CrossRef](#)]
47. Sayers, C.M.; den Boer, L.D. The elastic properties of clay in shales. *J. Geophys. Res. Sol. Ea.* **2018**, *123*, 5965–5974. [[CrossRef](#)]
48. Li, X.; Chen, K.; Li, P.; Li, J.; Geng, H.; Li, B.; Li, X.; Wang, H.; Zang, L.; Wei, Y.; et al. A New Evaluation Method of Shale Oil Sweet Spots in Chinese Lacustrine Basin and Its Application. *Energies* **2021**, *14*, 5519. [[CrossRef](#)]
49. Hashin, Z.; Shtrikman, S. A variational approach to the theory of the elastic behaviour of multiphase materials. *J. Mech. Phys. Solids* **1963**, *11*, 127–140. [[CrossRef](#)]
50. Berryman, J.G. Long-wavelength propagation in composite elastic media II. Ellipsoidal inclusions. *J. Acoust. Soc. Am.* **1980**, *68*, 1820–1831. [[CrossRef](#)]
51. Hudson, J.A. Overall properties of a cracked solid. *Math. Proc. Camb. Phil. Soc.* **1980**, *88*, 371–384. [[CrossRef](#)]
52. Domenico, S.N. Elastic properties of unconsolidated porous sand reservoirs. *Geophysics* **1977**, *42*, 1339–1368. [[CrossRef](#)]
53. Quakenbush, M.; Shang, B.; Tuttle, C. Poisson impedance. *Lead. Edge* **2006**, *25*, 128–138. [[CrossRef](#)]
54. Tian, L.X.; Zhou, D.H.; Lin, G.K.; Jiang, L.C. Reservoir prediction using Poisson impedance in Qinhuangdao, Bohai Sea. In *SEG Annual Meeting*; European Association of Geoscientists & Engineers: Denver, CO, USA, 2010.
55. Ming, J.; Qin, D.H. An effective method of fluid discrimination using Poisson impedance and multi-attribute inversion. In *SEG International Exposition and Annual Meeting*; Society of Exploration Geophysicists: Dallas, TX, USA, 2016.

56. Shang, F.; Xie, X.N.; Li, S.F. Enrichment conditions of Hetaoyuan Formation shale oil in Biyang Depression, China. *J. Pet. Explor. Prod. Technol.* **2019**, *9*, 927–936. [[CrossRef](#)]
57. Li, L.J.; Lyu, Q.Q.; Shang, F. Seismic prediction of lithofacies heterogeneity in paleogene hetaoyuan shale play, Biyang depression, China. *Open Geosci.* **2020**, *12*, 1383–1391. [[CrossRef](#)]
58. Mavko, G.; Mukerji, T.; Dvorkin, J. *The Rock Physics Handbook: Tools for Seismic Analysis in Porous Media*; Cambridge University Press: Cambridge, UK, 2009.

**Disclaimer/Publisher’s Note:** The statements, opinions and data contained in all publications are solely those of the individual author(s) and contributor(s) and not of MDPI and/or the editor(s). MDPI and/or the editor(s) disclaim responsibility for any injury to people or property resulting from any ideas, methods, instructions or products referred to in the content.